Current Optics and Photonics
Vol. 4, No. 1, February 2020, pp. 50-56

ISSN: 2508-7266(Print) / ISSN: 2508-7274(Online)
DOI: https://doi.org/10.3807/COPP.2020.4.1.050

Design of Concentrating System for Solar Side-pumped Slab Laser

Wentong Fan[1], Yan Liu[1]*, Pan Guo[1], Rui Deng[1], Nan Li[2], Fukang Ding[1], Yasha Li[3], Jun Zhou[4], and Shiwei Xie[1]

[1]*College of Science, China Three Gorges University, Yichang 443002, China*
[2]*School of Physics, Northeast Normal University, Changchun 130022, China*
[3]*College of Electrical Engineering & New Energy, China Three Gorges University, Yichang 443002, China*
[4]*Shanghai Institute of Optics and Fine Mechanics, Chinese Academy of Sciences, Shanghai 201800, China*

(Received October 30, 2019 : revised December 11, 2019 : accepted December 11, 2019)

The design of a concentration system for a solar side-pumped slab laser was investigated. The side size of the slab laser medium is 2 mm × 20 mm. Based on the principle of the edge ray, a secondary concentrating system consisting of a rectangular parabolic mirror (RPM) and a rectangular dielectric-filled compound parabolic concentrator (RDCPC) was demonstrated. The focal length of RPM is 1200 mm and the size is 734 mm × 2000 mm. The outlet size of the RDCPC is 2 mm × 20 mm. The concentration effect was analyzed by using Tracepro optical software. The results showed that the concentration efficiency reached 81.3% and the uniformity of the spot was 91.4% after optimization. This design of concentration system is of great reference value for a solar side-pumped slab laser.

Keywords : Solar pumped laser, Slab laser, Parabolic mirror, Dielectric-filled CPC
OCIS codes : (140.3580) Lasers, solid-state; (140.5560) Pumping; (350.6050) Solar energy

I. INTRODUCTION

With the development of society, traditional fossil energy can no longer meet needs, and the consumption of traditional fossil energy will bring a series of environmental problems. Therefore, the development and utilization of new clean energy has attracted worldwide attention. As an inexhaustible source of energy, solar energy has received more and more attention. As a kind of effective way to utilize solar energy, the solar-pumped laser has become one of the hot spots in the field of laser technology in recent years [1, 2]. Solar pumped lasers have great prospects in fields of space solar powered stations, space laser communication, laser propulsion, military and photochemistry [3].

The pumping configuration of solar lasers can be divided into end-pumping, side-pumping and hybrid-pumping. Concentrating systems also can be imaging or non-imaging optical systems. Solar end-pumping was adopted earlier [4]. In 1992, Dave Cooke used a telescope mirror as a first-stage concentrator for end-pumping, which achieved a laser output of more than 3 W [5]. A Fresnel lens was used to achieve the end-pumping of the solar laser in 2007. The output power was 24.4 W [6]. In 2009, Jianwei He reported a solar end-pumped Nd:YAG laser of which the concentrator was also a Fresnel lens [7].

Side-pumping is also a common pumping method. In 2003, Lando reported a solar side-pumped laser with concentrator composed of a primary mirror and a two-dimensional CPC. The output power was 46 W [8]. In 2014, Dawei Liang demonstrated a concentration system consisting of four Fresnel lens-folding mirrors, four fused quartz crystals, four 2D-CPC and four V-shaped cavities to realize the side-pumping of a Nd:YAG laser rod. The output power was 59.1 W through theoretical analysis [9]. In 2016, Dawei Liang reported a concentration system which was composed of a heliostat-parabolic mirror, an ellipsoidal fused silica concentrator and a 2V-shaped pumping cavity. The output power of TEM_{00}-mode is 4.5 W [10]. In 2017, S. Mehellou used a heliostat-parabolic mirror system, twisted optical waveguide, 2D-CPC and

*Corresponding author: liuyan703@163.com, ORCID 0000-0003-2806-9264
Color versions of one or more of the figures in this paper are available online.

V-shaped cavity to pump the side of the laser rod, resulting in a 2.7 W laser output [11]. In 2019, 5.40% slope efficiency of a solar laser was achieved by side-pumping of a 3 mm diameter, 30 mm length Nd:YAG crystal rod with a concentration system which was composed of a heliostat-parabolic mirror, a fused silica aspheric lens, and a two-dimensional semi-cylindrical pump cavity [12].

Hybrid-pumping is also an effective method if the concentration efficiency of end-pumping or side-pumping is not high enough. In 2013, J. Almeida demonstrated a concentration system consisting of a heliostat-parabolic mirror, a conical-shaped light guide, a 3D-CPC and a conical cavity to pump the laser crystal and a laser output of 40 W was obtained [13]. In 2015, J. Almeida used a cone-shaped fused silica lens to further converge sunlight from heliostat-parabolic mirror into a conical pump chamber and 56 W laser output power was obtained [14]. In 2016, Dawei Liang used a parabolic concentration system, a fused silica aspheric lens and a conical pump cavity to pump the Nd:YAG laser rod. The CW laser output reached 29.3 W [15]. In 2017, 37.2 W continuous-wave multimode laser output was also demonstrated with this concentration system [16]. In 2018, Dan Fang obtained a laser output of 3.5 W with a concentration system consisting of a Fresnel lens, conical condenser and conical pump cavity [17]. In 2018, Z. Guan reported a solar concentration system which was composed of a Fresnel lens and a gold-plated conical pumped cavity. 33.1 W continuous wave output laser power was obtained [18]. In 2019, Vistas achieved a 24 W multimode laser output through a concentration system consisting of a heliosta-parabolic mirror system, a fused silica liquid light guide lens and a conical pump cavity [19].

However, for the high-power solid-state lasers based on cylindrical laser rod, high temperature at the central axis and a serious thermal effect can make beam quality worse [20, 21]. So, reducing the thermal effects becomes a major problem to be solved in order to meet the requirements of high power and high beam quality in laser output [22]. Because the temperature gradient occurs in the thickness direction of the slab, the thermal lens effect and the thermo-optical distortion effect can be reduced substantially in the slab laser, and the laser output power would be improved greatly [23]. However, the difficulty of designing the concentrator increases because the thickness of the slab is smaller than the diameter of the laser rod. In order to realize the solar side pumping of a slab laser, in this paper, a two-stage concentration system composed of RPM and RDCPC is proposed to collect solar radiation on the side of the slab Nd:YAG crystal.

II. DESIGN PRINCIPLE

The structure of the solar slab laser concentration system proposed in this paper is shown in Fig. 1. The concentration system consists of an RPM and an RDCPC. The

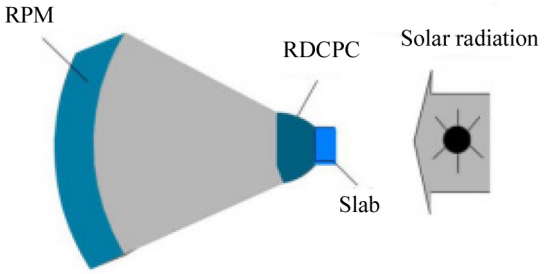

FIG. 1. Structure of concentration system for solar side-pumped slab laser.

slab-shaped gain medium was placed behind the RDCPC. The direction of solar radiation is parallel to the axis of the parabolic mirror.

The non-imaging concentration system of the solar side-pumped slab laser was designed according to the principle of the edge ray. The concentrating efficiency and the uniformity of the converging spot were mainly considered. The design method of concentration system is as follows: (1) The outlet size of the secondary concentrator is 2 mm × 20 mm, which is the same as the side of the slab laser medium. (2) The edge ray reaching the primary concentrator is reflected to the inlet of the secondary concentrator. (3) The secondary concentrator called rectangular dielectric-filled compound parabolic concentrator (RDCPC) needs to converge the light as much as possible to the outlet. It requires the RDCPC not only has the larger inlet area, but also has a larger maximum acceptance angle.

The RPM is used as the first-stage concentrator. Compared with a transmission concentrator (such as a Fresnel lens), the dispersion is not considered in the design and only the divergence angle of the sunlight needs to be considered. Dispersion has a great influence on the concentrating effect of the Fresnel lens. For example, the sunlight passes through a rectangular Fresnel lens based on the material of PMMA, and the focal length, groove pitch, thickness and size of the Fresnel lens are 1200 mm, 0.33 mm, 3 mm, 1400 mm × 1050 mm, respectively. Because of the dispersion, the spot on the focal plane of the Fresnel lens is larger and it makes the concentration efficiency lower. Even if the laser rod has a radius of 7 mm, the total concentration efficiency is only 50% [24].

III. THE DESIGN OF THE CONCENTRATION SYSTEM

3.1. The Design of the Primary Concentrator

As shown in Fig. 2, incident sunlight has a divergence angle of 32'. It was reflected by a parabolic mirror to form a spot. The Eq. (1) was obtained from the parabolic equation:

$$d = \frac{r^2}{4f}. \tag{1}$$

The following equations can be obtained from the geometric relationship and the law of reflection:

$$\varphi = \arctan\left(\frac{r}{f-d}\right) + \delta, \tag{2}$$

$$h = (f-d) \times (\tan\varphi - \tan(\varphi - 2\delta)). \tag{3}$$

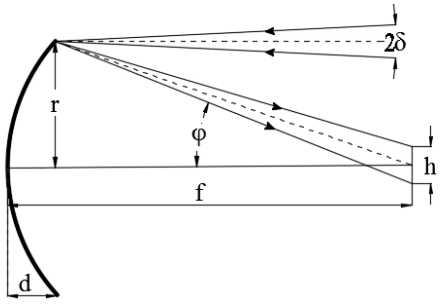

FIG. 2. Converging spot of sunlight passing through parabolic mirror.

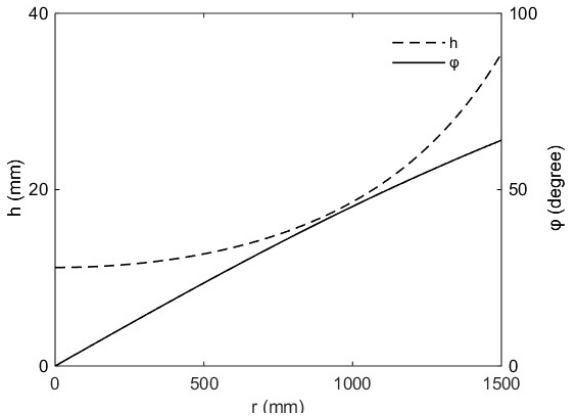

FIG. 3. Angle φ and focus spot diameter have a function of the radius of the parabolic mirror.

where φ is the included angle between the edge light reflected by the parabolic mirror and the central axis, h is the diameter of the focused spot, r is the radius of the parabolic mirror, and d is the height of the parabolic mirror. δ is the half-divergence angle of sunlight and its value is 16'. The focal length of the parabolic mirror is set to 1200 mm.

The relationship between the h, φ and r was shown in Fig. 3. The spot diameter h and angle φ increase as the radius of the parabolic mirror increases. The spot diameter h increases slowly when r is in the range of 0~1000 mm, and h increases quickly when r is in the range of 1000~1500 mm. If the parabolic mirror is circular, the reflection angle φ is constant. It is not conducive to the further compression of the spot by the secondary concentrator. Considering the size of the pumping surface of the slab laser, an RPM with a size of 734 mm × 2000 mm acted as the primary concentrator.

The concentrating effect was simulated with TracePro optical software. The irradiation map of the focal spot is shown in Fig. 4 with the sunlight passing through the primary concentrator. The focused spot is approximately elliptical. If a 2 mm × 20 mm receiving surface is placed on the focal plane, the concentration efficiency is only 21.9%. It obviously cannot meet the requirements by using only a primary concentrator, so it is necessary to add a secondary concentrator for further condensing.

3.2. The Design of the Secondary Concentrator

The parameters of a CPC include the outlet radius *a*, the inlet radius b, the concentrator length L, and the maximum acceptance half angle θ. The relationship of parameters is shown as follows:

$$\sin\theta = a/b. \tag{4}$$

If the maximum acceptance half angle of the CPC and the outlet radius were given, the radius of the inlet can be calculated by the above formula. The structure of the entire CPC can be obtained.

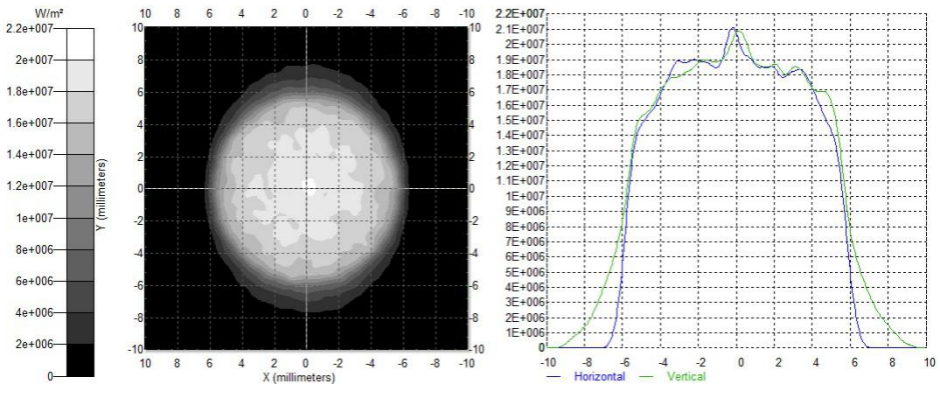

FIG. 4. Irradiation map of the focal spot.

It can be seen from Fig. 3 that the spot diameter h is 18.6 mm and the angle φ is 45.5° when the sunlight passes through the edge of the RPM with a width of 2000 mm. The spot diameter h is 12.0 mm and the angle φ is 17.7° when the sunlight passes through the edge of the RPM with a width of 734 mm. Obviously, the size and uniformity of the spot in two directions need to be further improved. In order to realize the solar side-pumped slab laser, the outlet of the CPC was set to rectangular. The rectangular compound parabolic concentrator (RCPC) as the secondary concentrator was proposed first.

In order to match the outlet size of the secondary concentrator with the pump side of the slab, the outlet of the RCPC can be set to a rectangle of 2 mm × 20 mm. When the outlet size of the RCPC is determined, there are two design methods for the structure of the RCPC. One is to calculate the inlet size of the RCPC by regarding the angle of φ as the maximum acceptance half angle θ of the RCPC. The other method is to calculate the maximum acceptance half angle θ of the RCPC by using the size of the spot on the focal plane as the RCPC inlet size. The essence of the above two methods is the same. Since the first method is relatively intuitive by comparing the inlet diameter of the RCPC with the spot diameter, the first method is adopted in the following design.

The relationship between inlet radius r_0 and the maximum acceptance half angle θ of the CPC is shown in Fig. 5. The maximum acceptance half angle of the CPC changes from 5° to 60°. When the CPC outlet radius is 1 mm, the corresponding angle φ is 17.7°. That is to say, the CPC maximum acceptance half angle θ is 17.7° and the corresponding CPC entrance diameter is 6.6 mm. It is smaller than the corresponding focal spot diameter h of 12.0 mm. When the outlet radius of CPC is 10 mm, the corresponding angle φ and the CPC maximum acceptance half angle θ were 45.5°. The CPC entrance diameter is 28.0 mm, and it is larger than the spot diameter h of 18.6 mm. It was shown that a large number of rays of sunlight reaching the focal plane cannot enter into the RCPC. This will lead to a decrease of the concentration efficiency.

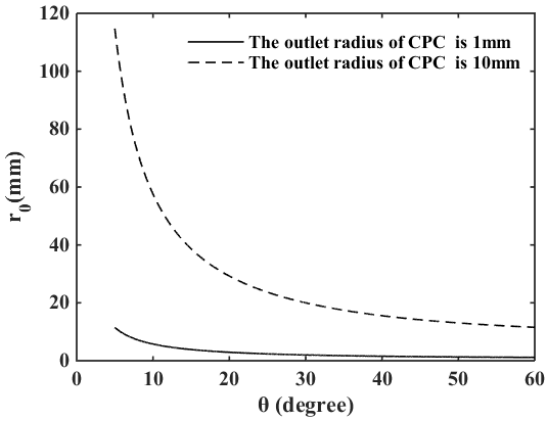

FIG. 5. Relationship between the inlet radius of the CPC and the maximum acceptance half angle.

In order to solve this problem, the RDCPC filled with BK7 was proposed. The relationship between the inlet radius of this DCPC and the maximum acceptance half angle is shown in Fig. 6. Comparing Fig. 5 with Fig. 6, it can be seen that when the outlet radius and the maximum acceptance half angle are the same, the inlet radius of the DCPC is significantly larger than that of the conventional CPC. When the outlet radius of the DCPC is 1 mm, the corresponding angle φ is 17.7° and the maximum acceptance half angle θ inside the DCPC is only 11.5°. At this time, it can be concluded that the inlet diameter of the DCPC is 10.0 mm, which is slightly smaller than the corresponding focal spot diameter of 12.0 mm. When the outlet radius of the CPC is 10 mm ,the corresponding edge angle φ is 45.5° and the maximum acceptance half angle inside the DCPC is 28.0°. The CPC entrance diameter is 42.6 mm, and it is larger than the corresponding focal spot diameter of 18.6 mm. According to the above discussion, the entrance size of the RDCPC in two directions can be obtained, respectively. Due to the advantages of reducing the manufacturing cost and increasing the maximum acceptance angle by properly intercepting the CPC, the shorter one (i.e. calculated from the entrance width of the RDCPC) is selected as the length of the concentrator. The structure of the RDCPC is shown in Fig. 7.

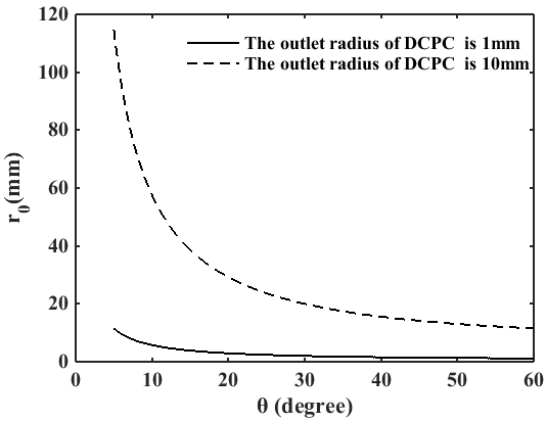

FIG. 6. Relationship between the inlet radius of the DCPC and the maximum acceptance half angle.

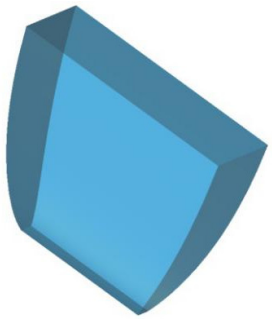

FIG. 7. Structure of the RDCPC.

The RDCPC with maximum internal acceptance angles of 28.0° and 11.5° and an outlet size of 20 mm and 2 mm in two directions was placed at the focal plane of the RPM, and the irradiation Map of the converging spot is shown in Fig. 8. It can be seen that the spot on the focal plane was compressed or stretched in two directions when the sunlight passed through the RDCPC. The shape of the converging spot was changed from oval to rectangular. The results show that the total concentrating efficiency of the concentration system is 69.6% and the uniformity of spot is 92.7%.

IV. OPTIMAL DESIGN

Because the short side of the outlet was used to calculate the length of the RDCPC, optimal intercepted length can be obtained by changing the maximum acceptance half angle in the other direction. Concentrating efficiency and uniformity of spot were shown in Fig. 9 through ray tracing. The maximum acceptance half angle changes from 25° to 70°. Three kinds of different refractive index optical glass including BK7, BK10 and F13 are acted as the filling material of the RDCPC.

The relationship between the concentrating efficiency and θ was shown in the Fig. 9. when θ is the same, the concentrating efficiency of the RDCPC with the filling medium F13 is the highest, and the concentrating efficiency of the filling medium BK10 is the lowest. The change trends of concentrating efficiency of the three materials is consistent with the change of θ. At first, they increase fast, then the increase rate is slightly slower. The efficiency decreases after reaching the maximum. The maximum concentration efficiency of RDCPC filled with F13, BK7 and BK10 were 90.3%, 89.7% and 89.6%, respectively. It also can be seen from Fig. 9 that the uniformity of the spot of the three kinds of RDCPC is relatively flat with the change of θ at first. It decreases slightly in the range of θ of 33 to 40 degree and then starts to increase. Considering the concentrating efficiency and the uniformity of the spot, the RDCPC with BK7 as the filling medium and 44 degree as the maximum acceptance half angle corresponding to the long side was finally selected as the optimized secondary concentrator.

The irradiation map of the receiving surface after the optimized concentration system was shown in Fig. 10. The concentrating efficiency is 81.3%, which is 11.7% higher than that before optimization which was mentioned in

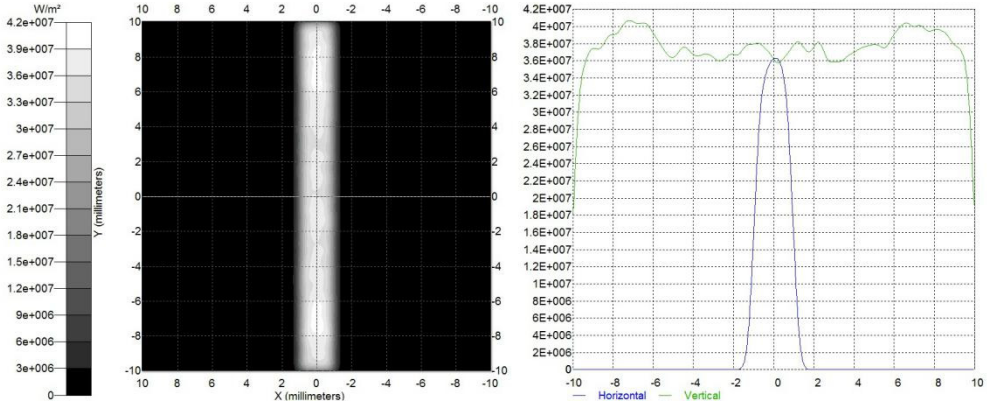

FIG. 8. Irradiation map of converging spot at the outlet of RDCPC.

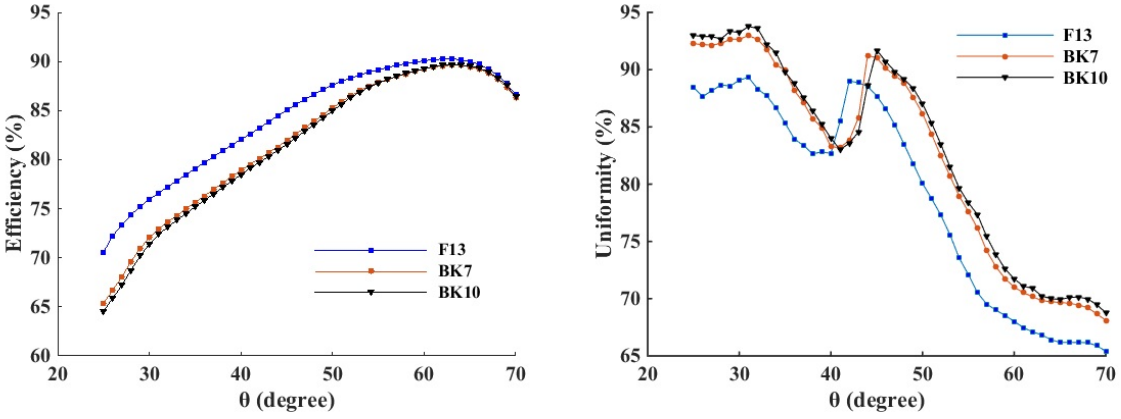

FIG. 9. The concentrating efficiency of the RDCPC and the uniformity of the spot change with the maximum acceptance half angle.

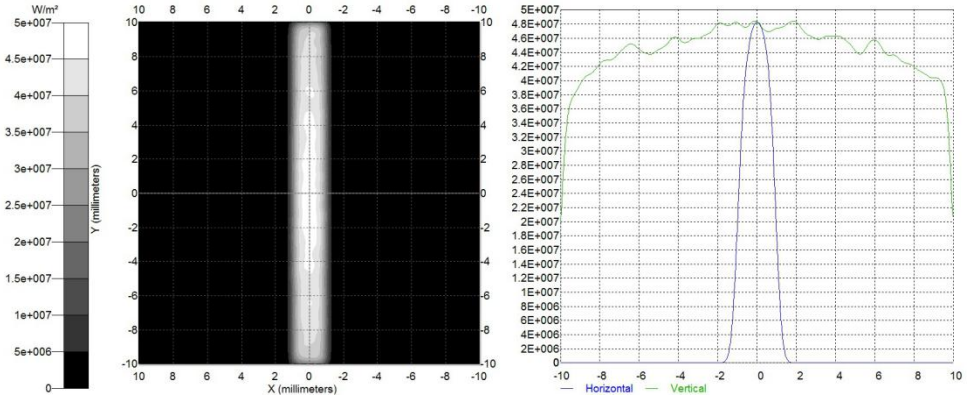

FIG. 10. Irradiation map of the converging spot after optimization.

Section 3; the uniformity of the spot is 91.2%, which is 1.5% lower than that before optimization. The optimized concentration system improves the concentrating efficiency on the basis of ensuring the uniformity of the spot.

The simulation shows that the concentrating efficiency and uniformity of the spot will decrease if the direction of solar radiation is not parallel to the axis of the parabolic mirror.

V. CONCLUSION

In this paper, a two-stage concentration system for a solar side-pumped slab laser was reported. The system consists of two parts, an RPM with a size of 734 mm × 2000 mm as a first-stage concentrator and an RDCPC with outlet size of 2 mm × 10 mm as a secondary concentrator. The concentrating effect of three kinds of RDCPC based different refractive index filling media of BK7, BK10 and F13 were compared. After optimization, the ideal result is obtained. After the sunlight passes through the concentration system, the concentration efficiency is 81.3% and the uniformity of spot is 91.2%. This kind of concentration system can also be suitable for the other solar side-pumped solid-state laser.

ACKNOWLEDGMENT

This work is supported by grant from Shanghai Key Laboratory of All Solid-state Laser and Applied Techniques Foundation Program (2013ADL02), Research Fund for Excellent Dissertation of China Three Gorges University (2019SSPY148).

REFERENCES

1. J. Almeida, D. Liang, and E. Guillot, "Improvement in solar-pumped Nd:YAG laser beam brightness," Opt. Laser Technol. **44**, 2115-2119 (2012).
2. Y. Suzuki, H. Ito, T. Kato, L. T. A. Phuc, K. Watanabe, H. Terazawa, K. Hasegawa, T. Ichikawa, S. Mizuno, A. Ichiki, S. Takimoto, A. Ikesue, Y. Takeda, and T. Motohiro, "Continuous oscillation of a compact solar-pumped Cr, Nd-doped YAG ceramic rod laser for more than 6.5 h tracking the sun," Sol. Energy **177**, 440-447 (2019).
3. H. Arashi and Y. Kaneda, "Solar-pumped laser and its second harmonic generation," Sol. Energy **50**, 447-451 (1993).
4. M. Weksler and J. Shwartz, "Solar-pumped solid-state lasers," IEEE J. Quantum Electron. **24**, 1222-1228 (1988).
5. D. Cooke, "Sun-pumped lasers:revisiting and old problem with nonimaging optics," Appl. Opt. **31**, 7541-7546 (1992).
6. T. Yabe, T. Ohkubo, S. Uchida, K. Yoshida, M. Nakatsuka, T. Funatsu, A. Mabuti, A. Oyama, K. Nakagawa, T. Oishi, K. Daito, B. Behgol, Y. Nakayama, M. Yoshida, S. Motokoshi, Y. Sato, and C. Baasandash, "High-efficiency and economical solar-energy-pumped laser with Fresnel lens and chromium codoped laser medium," Appl. Phys. Lett. **90**, 261120 (2007).
7. J. W. He, C. M. Chang, S. H. Yang, A. Ding, and L. W. Zhang, "Solar pumped Nd:YAG laser," Chin. J. Laser **36**, 255-256 (2009).
8. M. Lando, J. Kagan, B. Linyekin, and V. Dobrusin, "A solar-pumped Nd:YAG laser in the high collection efficiency regime," Opt. Commun. **222**, 371-381 (2003).
9. D. Liang, J. Almeida, and C. R. Vistas, "Scalable pumping approach for extracting the maximum TEM_{00} solar laser power," Appl. Opt. **53**, 7129-7137 (2014).
10. D. Liang, J. Almeida, C. R. Vistas, M. Oliveira, F. Goncalves, and E. Guillot, "High-efficiency solar-pumped TEM_{00}-mode Nd:YAG laser," Sol. Energy Mater. Sol. Cells **145**, 397-402 (2016).
11. S. Mehellou, D. Liang, J. Almeida, R. Bouadjemine, C. R. Vistas, E. Guillot, and F. Rehouma, "Stable solar-pumped TEM_{00}-mode 1064 nm laser emission by a monolithic fused silica twisted light guide," Sol. Energy **155**, 1059-1071 (2017).
12. D. Liang, C. R. Vistas, J. Almeida, B. D. Tiburcio, and D. Garcia, "Side-pumped continuous-wave Nd:YAG solar laser with 5.4% slope efficiency," Sol. Energy Mater. Sol. Cells **192**, 147-153 (2019).
13. J. Almeida, D. Liang, E. Guillot, and Y. Abdel-Hadi, "A 40 W cw Nd:YAG solar laser pumped through a heliostat:

a parabolic mirror system," Laser Phys. **23**, 065801 (2013).
14. J. Almeida, D. Liang, C. R. Vistas, and E. Guillot, "Highly efficient end-side-pumped Nd:YAG solar laser by a heliostat-parabolic mirror system," Appl. Opt. **54**, 1970-1977 (2015).
15. D. Liang, J. Almeida, and C. R. Vistas, "25 W/m^2 collection efficiency solar-pumped Nd:YAG laser by a heliostat-parabolic mirror system," Appl. Opt. **55**, 7712-7717 (2016).
16. D. Liang, J. Almeida, C. R. Vistas, and E. Guillot, "Solar-pumped Nd:YAG laser with 31.5 W/m^2 multimode and 7.9 W/m^2 TEM$_{00}$-mode collection efficiencies," Sol. Energy Mater. Sol. Cells **159**, 435-439 (2017).
17. D. Fang, X. H. Wang, F. Wang, and S. N. Liu, "Solar pumped Nd:YAG laser," Optik **124**, 3367-3370 (2013).
18. Z. Guan, C. Zhao, J. Li, D. He, and H. Zhang, "32.1 W/m^2 continuous wave solar-pumped laser with a bonding Na:YAG/YAG rod and a Fresnel lens," Opt. Laser Technol. **107**, 158-161 (2018).
19. C. R. Vistas, D. Liang, J. Almeida, B. D. Tiburcio, and D. Garcia, "A doughnut-shaped Nd:YAG solar laser beam with 4.5 W/m^2 collection efficiency," Sol. Energy **182**, 42-47 (2019).
20. R. Bouadjemine, D. Liang, J. Almeida, S. Mehellou, C. R. Vistas, A. Kellou, and E. Guillot, "Stable TEM$_{00}$-mode Nd:YAG solar laser operation by a twisted fused silica light-guide," Opt. Laser Technol. **97**, 1-11 (2017).
21. Z. Huang. "Theoretical optimization of output power in side pumped Nd^{3+}:YAG solar laser," Opt. Laser Technol. **111**, 592-596 (2019).
22. W. A. Clarkson, "Thermal effects and their mitigation in end-pumped solid-state lasers," J. Phys. D: Appl. Phys. **34**, 2381-2395 (2001).
23. T. Kane, R. Eckardt, and R. Byer. "Reduced thermal focusing and birefringence in Zig-zag slab geometry crystalline lasers," IEEE J. Quantum Electron. **19**, 1351-1354 (1983).
24. H. Pian, L. Yan, Z. Shuguang, C. Xuerong, Z. Jun, F. Shengqin, and S. Xiaotao,, "The influence of compound parabolic concentrator parameters on the solar laser condensation efficiency," Laser J. **38**, 8-11 (2017).